Analyse d'échangeurs convectifs contre-courant par modes de Graetz généralisés

Jules DICHAMP[1], Frédéric DE GOURNAY[2*], Franck PLOURABOUÉ[1]

[1]Institut de Mécanique des Fluides de Toulouse (IMFT) - Université de Toulouse, CNRS-INPT-UPS
Toulouse FRANCE
[2]Institut de Mathématiques de Toulouse, CNRS and Université Paul Sabatier
Toulouse, FRANCE
*(auteur correspondant : fplourab@imft.fr)

Résumé - Dans ce travail nous avons effectué une analyse systématique du transfert de chaleur dans un échangeur convectif contre-courant tridimensionnel en tenant pleinement compte de l'influence des entrées/sorties ainsi que la conduction longitudinale dans l'échangeur. L'analyse, menée pour des fluides aux propriétés constantes en utilisant une décomposition en mode de Graetz généralisée, étudie l'influence de la conductivité fluide/solide, la convection imposée, les conditions d'entrées/sorties à champ lointain, ainsi que les conditions au bord latérales. Dans tous les cas, nous trouvons un Péclet optimal pour les rendements chauds et froids. Cette étude ouvre de nouvelles perspectives pour les micro-échangeurs thermiques où une convection modérée permet de conjuguer efficacité et compacité.

Nomenclature

$V_{H,C}$ average velocity hot/cold tube, $\mathrm{m/s}$
$Pe \equiv \dfrac{\rho c V (2R)}{k^F}$ Péclet number
$L^\star$ dimensionless exchanger length
k^F fluid thermal conductivity, $\mathrm{m^2/s}$
k^S solid thermal conductivity, $\mathrm{m^2/s}$
T temperature, K
$T^\star$ dimensionless temperature
$\epsilon_H \equiv \frac{T_H^{-\infty} - T_H^{+\infty}}{T_H^{-\infty} - T_C^{+\infty}}$ hot effectiveness
$\epsilon_C \equiv \frac{T_C^{-\infty} - T_C^{+\infty}}{T_H^{-\infty} - T_C^{+\infty}}$ cold effectiveness
$T_{H,C}^{\pm\infty}$ Temperature at $\pm\infty$ in hot/cold tubes, K
R tube radius, m

1. INTRODUCTION

Conjugate counter-flow heat-exchangers are widely used in thermal and bluilding energy, chemical, and many other industrial applications [15]. In those applied contexts, most of the exchangers are designed with the help of lumped methods, such as the traditional Log Mean Temperature Difference (LMTD) method, compartmental or transverse average approximations, in order to predict and elaborate dedicated look-up tables and graphs for each precise configuration [15, 1].

It is important to take into account longitudinal conduction in regions where convective effects are not dominant. Indeed, longitudinal conduction effects were found significant for Péclet number as large as 100 in tubes [16, 10]. But this is even more crucial inside the solid domain of an exchanger, since, in the solid part longitudinal and transverse conduction are of similar magnitude. This is especially true in configurations where solid walls are not thin, as opposed to fin exchangers, where a simple thermal resistance model to couple inlet and outlet fluids compartments with solid conduction is not precise enough.

Since, generically, the local transfer rate from the fluid into the solid is found to abruptly decay from the inlet along the longitudinal direction [5, 20], a strong emphasis has to be made upon the influence of the inlet and outlet conditions. To be more specific, in many cases a fully

developed thermal boundary outlet condition is chosen [21, 22, 18, 19, 14, 20] to model downstream convection. This is consistent with convectively dominated situations with very large Péclet number. For more moderate Péclet numbers, a more elaborate coupling of the exchanger with the inlet/outlet is needed to properly take into account the influence of the convection leak inside the outlet, as well as the possible upstream back-conduction in the inlet.

The aim of this contribution is so to further explore the influence of inlet/outlet coupling and longitudinal conduction onto a counter-current exchanger both in the balanced and unbalanced configuration using a numerical implementation

2. Governing Problem

We consider laminar convection-conduction arising in a fluid having constant properties. In the following we assume that the hot and cold tubes are filled with the same fluid, although this simplifying assumption is not a restriction of the proposed approach. **However it must be pointed out that unsteadiness turbulent flow are not cover by the presented approach.**

Fully developed solution of Navier-Stokes momentum equations in cylindrical tubes oriented along direction z are given by the Poiseuille longitudinal velocity $\mathbf{v}_{H,C} = v_{H,C}(r)\,\mathbf{e}_z = \pm(3V_{H,C}/2)\,(1-(r/R)^2)\;\mathbf{e}_z$ where V_H —resp. V_C– stands for the average velocity in the hot — resp. cold — tube, where R is the tube radius and $\mathbf{e}_z$ is the unit vector along z direction.

Following previous studies (e.g [14]), let us now define the stationary flux balance in three dimensions for **the dimensionless temperature** $T^\star = \dfrac{T-T_H^{-\infty}}{T_H^{-\infty}-T_C^{+\infty}} + \dfrac{T-T_C^{+\infty}}{T_H^{-\infty}-T_C^{+\infty}}$

$$\begin{array}{rlcll} Pe_{H,C}v^\star(\xi^\star)\partial_{z^\star}T^\star - & (\partial^2_{x^\star}+\partial^2_{y^\star}+\partial^2_{z^\star})T^\star & = & 0, & \text{in} \quad \text{Fluid} \\ & (\partial^2_{x^\star}+\partial^2_{y^\star}+\partial^2_{z^\star})T^\star & = & 0, & \text{in} \quad \text{Solid} \end{array} \tag{1}$$

$T_H^{-\infty}$ —resp. $T_C^{+\infty}$— stands for hot —resp. cold— homogeneous temperature in hot —resp. cold— inlet tube for $z \to -\infty$ —resp. $z \to +\infty$—. Those temperatures are datas of the problem. Outlet homogeneous temperatures $T_H^{+\infty}$ —resp. $T_C^{-\infty}$— stands for the hot —resp. cold — homogeneous temperature outlet at $z \to +\infty$ —resp. $z \to -\infty$—. Those temperatures are unknowns of the problem and must be computed.

In most of the following we consider the special case of balanced counter-current configuration where longitudinal velocities are identical in $U_H = U_C = U$ and using the same fluid in the hot and cold tubes as well as antisymetric input temperature conditions $T_H^{\star-\infty} = -T_C^{\star+\infty} = 1$ (antisymetry given by the choice of dimensionless temperature which have been translated).

The solid part of the exchanger is associated with a conductivity k^S and the fluid part with conductivity k^F.

Hot/Cold inlet/outlet tubes fulfill lateral homogeneous Neumann boundary conditions whereas the exchanger is subjected to lateral Robin boundary condition. A schematic perspective view of a full exchanger is shown in Figure 1 **(b)**

3. Mathematical analysis and numerical implementation

Main equation (1) refers as the extended Graetz problem which is an extension of a classical class of PDE problems in which one can decompose the temperature field on a basis of eigenvalues and eigenvectors which are called in the literature Graetz modes and Graetz eigenvalues. On previous contributions [12, 13, 6] it was proven that equation (1) on general configurations

can be written with the following ODE

$$\frac{d}{dz}\phi(z) = A\,\phi(z) \tag{2}$$

with operator A defined as

$$A \;=\; \begin{pmatrix} \tilde{v}^\star & -(\partial^2_{x^\star} + \partial^2_{y^\star}) \\ 1 & 0 \end{pmatrix}, \;\text{ with }\; \phi = \begin{pmatrix} \partial z^\star T^\star \\ T^\star \end{pmatrix} \tag{3}$$

and that matrix A satisfies self-adjointness and compacity which allows a similar spectral decomposition as in classical case. Following this mathematical framework, a numerical method based on Graetz modes was developed in [11]. Since we use a generalyzed Graetz-mode decomposition, all longitudinal variations are analytically known. To be more specific, temperature in each hot/cold inlet/outlet tubes and in the exchanger writes as

$$\begin{array}{lcll} T^\star(\xi^\star, z^\star) & = & \sum_{\mathbb{N}^*} x_n^+ T_n^+(\xi^\star) e^{\lambda_n^+ z^\star} + x_n^- T_n^-(\xi^\star) e^{\lambda_n^-(z^\star - L/R)} & \text{exchanger } z^\star \in [0, L] \\ T^\star(\xi^\star, z^\star) & = & x_0^H + \sum_{\mathbb{N}^*} x_n t_n^+(\xi^\star) e^{\mu_n^+(z^\star - L/R)} & \text{hot outlet tube } z^\star \geq L/R \\ T^\star(\xi^\star, z^\star) & = & x_0^C + \sum_{\mathbb{N}^*} x_n t_n^-(\xi^\star) e^{\mu_n^- z^\star} & \text{cold outlet tube } z^\star \leq 0 \\ T^\star(\xi^\star, z^\star) & = & 1 + \sum_{\mathbb{N}^*} x_n t_n^-(\xi^\star) e^{\mu_n^- z^\star} & \text{hot inlet tube } z^\star \leq 0 \\ T^\star(\xi^\star, z^\star) & = & \frac{T_C^{+\infty}}{T_H^{-\infty}} + \sum_{\mathbb{N}^*} x_n t_n^+(\xi^\star) e^{\mu_n^+(z^\star - L/R)} & \text{cold inlet tube } z^\star \geq L/R \end{array} \tag{4}$$

with x_n the amplitudes of the modes, T_n the modes and λ_n the eigenvalues of operator A (positive or negative), $\mu_n^\pm$ are the classical Neumann Graetz eigenvalues in the inlet/outlets (also positive or negative). Then, providing continuity coupling conditions between hot/cold inlet/outlet tubes and the exchanger part, one can define a functional,

$$J_{\mathcal{L}_2}(T^\star) \;=\; \int\limits_{D_{0,L}^{H,C}} |T^\star_{left} - T^\star_{right}|^2 \,\mathrm{d}s + \int\limits_{D_{0,L}^{H,C}} |\partial_z T^\star_{left} - \partial_z T^\star_{right}|^2 \,\mathrm{d}s, \tag{5}$$

so that, minimizing (5) provides the stated continuity conditions. By decomposing the temperature field as shown in equation (4)), one can write the minimization problem as a linear system, as done in [11]

$$\mathbf{M}_{\mathcal{L}_2}\mathbf{x} \;=\; \mathbf{b} \tag{6}$$

Solving this system finally gives the temperature field in the entire domain. It is important to note that we do not numerically compute the longitudinal variations of the temperature field since they are analytically known. This means that the initial three-dimensional problem has been maped as a two-dimensionnal problem which ensure very low computational cost.

4. Results

Here, we mainly focused the discussion on hot and cold effectiveness defined as $\epsilon_H \equiv \frac{T_H^{\star -\infty} - T_H^{\star +\infty}}{T_H^{\star -\infty} - T_C^{\star +\infty}}$ and $\epsilon_C \equiv \frac{T_C^{\star -\infty} - T_C^{\star +\infty}}{T_H^{\star -\infty} - T_C^{\star +\infty}}$. $\epsilon_H = \epsilon_C$ in balanced configurations. **This symetric property of the hot/cold effectiveness can be used as a validation of the method. It is also possible to show that in the same case of a balanced configuration, the eigenvalues of the problem in the exchanger domain are anti-symetric ($\lambda_n^+ = -\lambda_n^-$), a property useful for a supplementary validation.**

A systematic exploration of the problem having seven dimensionless parameter has been performed. Here, we focus on the influence of the main parameters on the effectiveness. We

therefore explore the influence of the Péclet number, the exchanger dimensionless length $L^\star$, the conductivity ratio k^S/k^F, and the Biot number Bi (which is related to the lateral Robin boundary condition of the exchanger). In all cases we found an optimal Péclet number Pe^o for the effectiveness associated with moderate convection, i.e, $6 < Pe^o < 12$. **One can note that the Péclet range hereby investigated is rather small, but it is important to stress that it is not a restriction of the presented approach. The asymptotic limit for large Péclet where the convection dominates is a specific case. The choice of moderate Péclet was mainly done to closely investigate the effects of longitudinal conduction.**

When the Péclet number rises, so does the transfer performances, at the cost of very low effectiveness. Elongated exchangers reduce the lost of effectiveness but they also result in poor compactness. Performance degradation at high Péclet number are related to convective leaks at the outlets. Figure 1 **(a)**, display the behavior of hot effectiveness versus Péclet number, for various Biot numbers. One can observe an optimal effectiveness at moderate Péclet which is poorly sensitive to large Bi variations. Figure 1 **(c)** is the corresponding 2D longitudinal section in (x, z) plane of the temperature field at optimal Péclet for $Bi = 10^{-1}$.

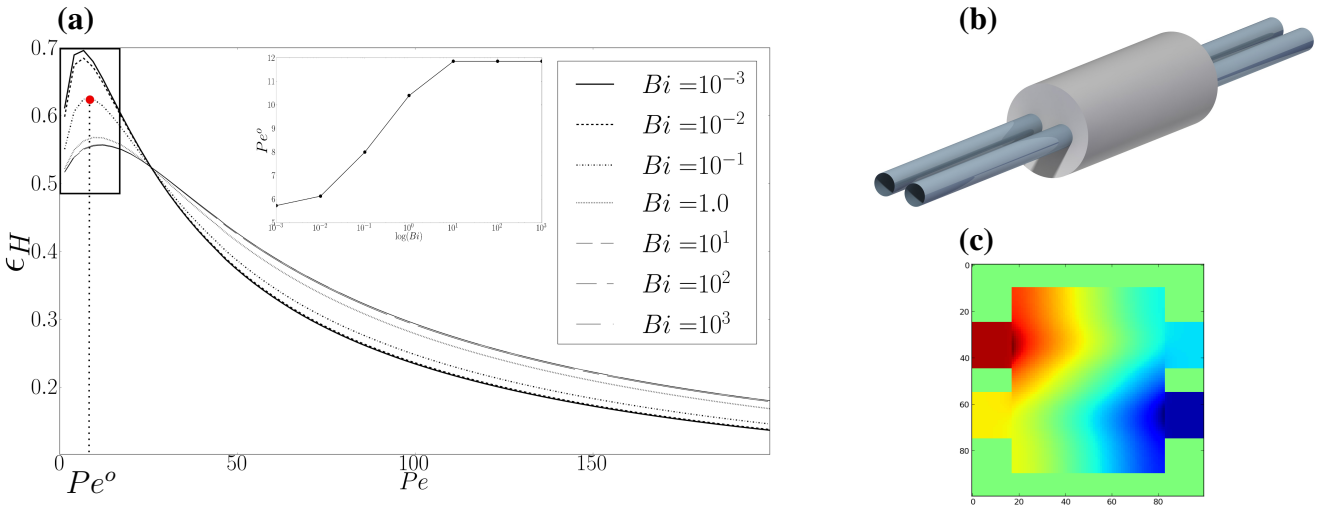

Figure 1: **(a)** Hot effectiveness against Péclet for $Bi = 10^{-3}, 10^{-2}, 10^{-1}, 1, 10^1, 10^2, 10^3$. Inset figure is Péclet at maxium hot effectiveness against $\log(Bi)$. **(b)** Perspective view using real size of full exchanger. **(c)** Longitudinal temperature fields at optimal Péclet on $Pe^o = 8$, $L^\star = 20$, $Bi = 10^{-1}$ (red dot in **(a)**). We have rescaled the horizontal $z^\star$ axis in order the inset figures to reach a 1 :1 aspect ratio.

4.1. Influence of exchanger length and convective leaks

Let us now consider the adiabatic limit of zero Biot number. Figure 2 **(a)** displays the exchanger effectiveness when the Péclet number is varied for various dimensionless lenght $L^\star$. All effectiveness curves display a similar behavior, with three distinct regimes : (i) a small increase at law Péclet numbers followed by (ii) an optimal effectiveness arising at moderate Péclet, and (iii) a monotonous decrease arising at large Péclet. It is worth mentioning that, as expected, the effectiveness improves as dimensionless lenght $L^\star$ increases, as shown in Figure 2 **(b)**, since the longer the exchanger, the better the transfer. Nevertheless, it is obvious that reaching $L^\star$ values larger than one hundred does not present good practical perspectives, for obvious cost and calibre limitations. Considering the already strongly elongated exchanger where $L^\star = 10$,

it is striking to observe how poorly efficient such exchanger can be for Péclet numbers not larger than one hundred, whilst in most practical situations the Péclet reaches much larger values (as large as several thousand at least). This statement has to be tempered with the fact that the hereby chosen exchanger geometry is obviously very far from the most efficient one.

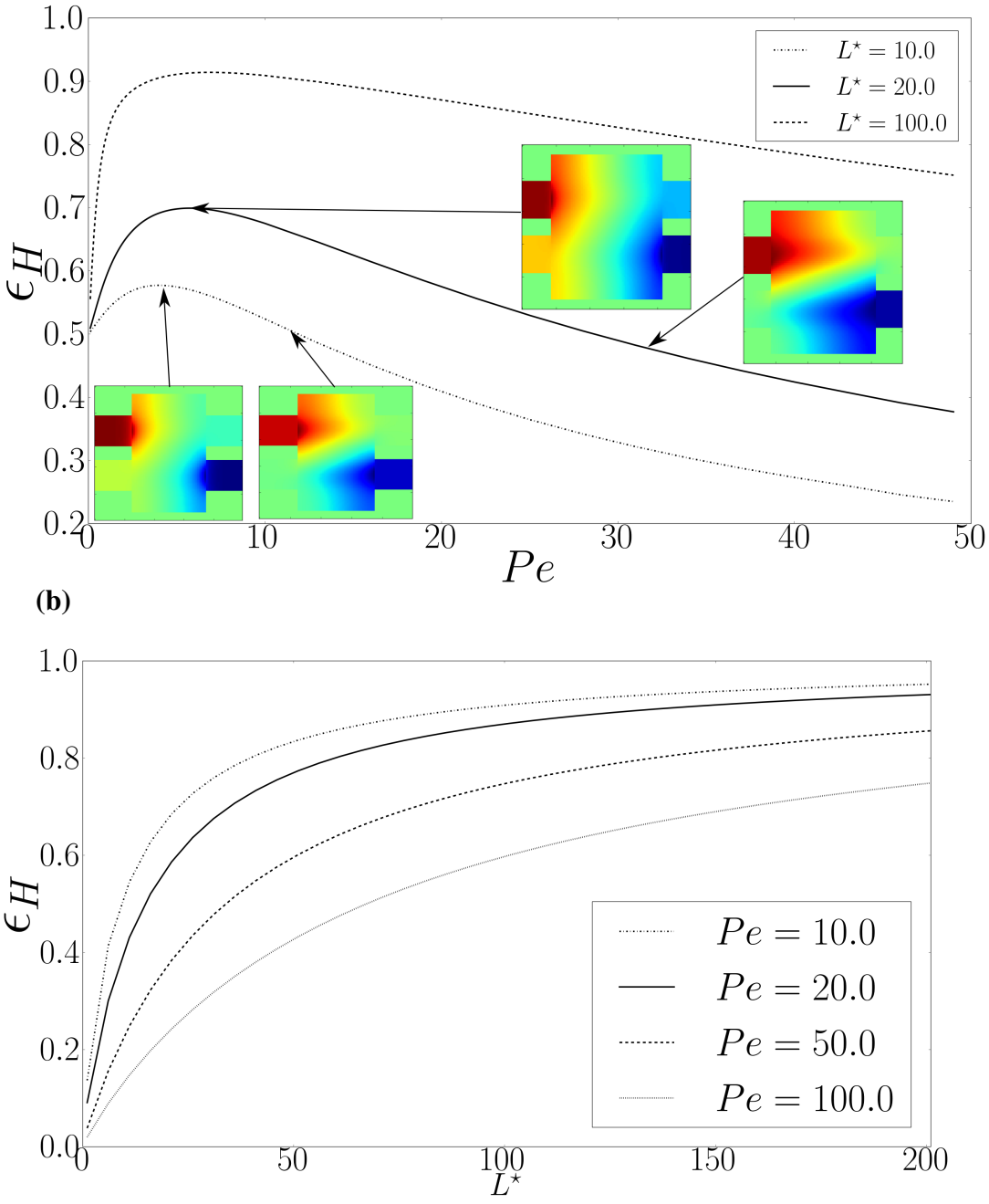

Figure 2: In the three figures $Bi \ll 1$, $\frac{k^S}{k^F} = 1$. **(a)** ϵ_H against Péclet for $L^\star = 10, 20, 100$. Inset figures represent the computed longitudinal temperature fields at the maximum hot effectiveness as well as when the convective leak is starting to rise. It is important to stress that the aspect ratio of the figure is not the actual one for obvious caliber constraints. We have rescaled the horizontal $z^\star$ axis in order the inset figures to reach a 1 :1 aspect ratio, **(b)** ϵ_H against $L^\star$ for $Pe = 10, 20, 50, 100$, **(c)** ϵ_H against Péclet rescaled by $L^\star$ for $L^\star = 10, 20, 50, 100$.

Nevertheless we believe that the reported qualitative observations are generic i.e, (i) an increasing effectiveness for small Péclet, (ii) some optimal effectiveness for moderate Péclet (iii) an effectiveness collapse at large Péclet. Obviously the larger the Péclet the larger the exchanges as later-on examined from the analysis of the Nusselt number. But this ineffectiveness is at the cost of an enlarged total injected energy to convect the fluids for the obtained transfer rate. Figure 2 **(a)** also provides some interesting insets representing the temperature field in the $(y^\star, z^\star)$ plane (rescaled along the $z\star$ direction to keep with a 1 :1 aspect ratio of the insets) illustrating the origin of the effectiveness collapse. As the Péclet is increased, a larger and larger fraction of the initial hot inlet temperature is progressively convected toward the outlet, without having the chance to be transferred into the cold one throught conduction within solid. This convective heat-leakage across outlets is the mechanism by which the exchanger effectiveness is inevitably degraded as one increases convection for raising total heat transfer.

4.2. Variation of conductivity ratio

Figure 3 **(b)** illustrates the influence of the conductivity aspect ratio when the solid has larger conductivity compare to the convected liquid. In most applications using solid metals, the solid is indeed a better heat conductor than the fluid. The observed transverse heat profile at the exchanger longitudinal middle plane ($z^\star = L^\star/2$) shows distinct regimes. For identical conductive properties in the fluid and the solid, i.e $k^S/k^F = 1$, the observed transverse gradients are spreading all around the fluids tube inside the solid (with anti-symmetric shape in the ($x^\star$,$y^\star$) plane in this balanced configuration). This illustrates that transverse conduction in the solid arises, in this case, with transverse variation comparable to the tube diameters. On the contrary, in Figure 3 **(b)** as k^S/k^F increases, the transverse conduction gradients in the solid shortens its typical length-scale variations to become more and more localyzed in the vicinity of the tubes frontiers $\mathcal{C}^E_{H,C}$, leaving an almost iso-thermal temperature field within the rest of the solid. Figure 3 **(a)** then shows that the optimal effectiveness is reached in the limit of large k^S/k^F. The small difference which is observed for the effectiveness curve between the case $k^S/k^F = 10^2$ and $k^S/k^F = 10^3$ indicates that there is an asymptotic maximum effectiveness associated with the limit $k^S/k^F \to \infty$. Both the iso-thermal behavior in the solid and the increasing effectiveness with increasing k^S/k^F ratio where to be expected. The more conductive the solid, the better the heat exchange between the fluids. Nevertheless, even for extremely large k^S/k^F ratio, the three regimes (*i*,*ii*,*iii*) are also recovered in Figure 3 **(a)**. This indicated that even though the solid is extremelly good conductor, the convective conditions (associated with Pe number) and the exchanger aspect ratio $L^\star$ are driving the effectiveness. Furthermore it is very interesting to observe that the optimal effectiveness arising at moderate Pe number is almost insensitive to the conductivity ratio parameter.

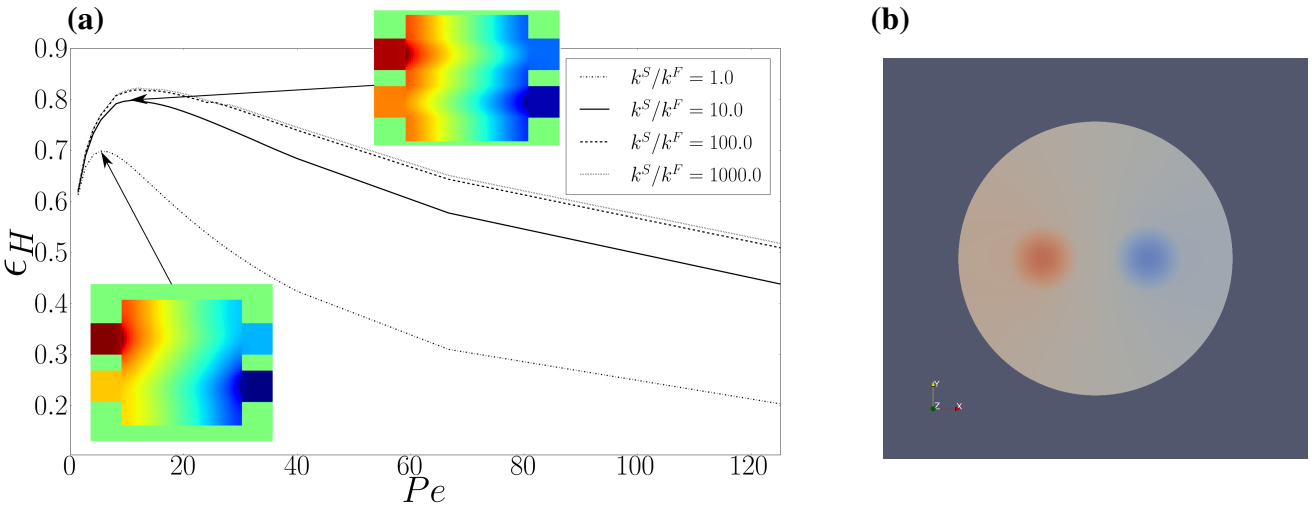

Figure 3: **(a)** ϵ_H against Péclet for $k^S/k^F = 1, 10, 100, 1000$ and $L^\star = 20$, $Bi = 10^{-6}$. Longitudinal temperature fields have been computed at the maxium hot effectiveness. $z^\star$ axis has been rescaled in order for the inset figures to reach a 1 :1 apsect ratio. **(b)** Transversal temperature fields in exchanger at $z^\star = \frac{L^\star}{2}$ for $L^\star = 20$, $Bi = 10^{-6}$ and $k^S/k^F = 10$

5. CONCLUSIONS

We have performed a systematic study of a parallel convective exchanger from analysing the influence of physical, mechanical, and thermal parameters Using a Generalyzed Graetz mode decompositions, we analyze the exchanger effciency and performance, in many operating conditions from exploring the dimensionless parameter space associated with Péclet number, Biot number, conductivity ratio, geometry aspect ratio, and operating temperature ratio.

We believe these results to be of general scope for many other counter- flow exchanger geometries. As a perspective, the use of Generalyzed Graetz mode decompositions could allow some systematic exploration of geometry exchanges properties.

Références

[1] J. C. Bradley. Counterflow, crossflow and cocurrent flow heat transfer in heat exchangers : analytical solution based on transfer units. *J Heat and Mass Transfer*, 46(4) :381–394, 2010.

[2] Y. P. Cheng, Z. G. Qu, W. Q. Tao, and Y. L. He. Numerical Design of Efficient Slotted Fin Surface Based on the Field Synergy Principle. *Numer. Heat Transfer, Part A*, 45(6) :517–538, 2004.

[3] R.C. Chu, R.E. Simons, M.J. Ellsworth, R.R. Schmidt, and V. Cozzolino. Review of Cooling Technologies for Computer Products. *IEEE Trans. Device Mater. Rel.*, 4(4) :568–585, 2004.

[4] W. Escher, B. Michel, and D. Poulikakos. Efficiency of optimized bifurcating tree-like and parallel microchannel networks in the cooling of electronics. *Int. J. Heat Mass Transfer*, 52(5-6) :1421–1430, 2009.

[5] W. Escher, B. Michel, and D. Poulikakos. A novel high performance, ultra thin heat sink for electronics. *Int. J. Heat Fluid Flow*, 31(4) :586–598, 2010.

[6] J. Fehrenbach, F. De Gournay, C. Pierre, and F. Plouraboué. The Generalized Graetz problem in finite domains. *SIAM. J. Appl. Math*, 72 :99–123, 2012.

[7] J. Fehrenbach, F. De Gournay, and F. Plouraboué. Shape optimization for the generalized Graetz problem . *Struct. Multidiscip. O.*, 49 :993–1008, 2014.

[8] H. Kobayashi, S. Lorente, R. Anderson, and A. Bejan. Serpentine thermal coupling between a stream and a conducting body. *J. Appl. Phys.*, 111(19-20) :044911, 2012.

[9] I. C. Mihai. Heat transfer in minichannels and microchannels CPU cooling systems.

[10] R. Nunge, E. W. Porta, and W.N. Gill. Axial conduction in the fluid streams of multistream heat exchangers. *Chem. Eng. Progr. Symp*, 63 :80 ?91, 1967.

[11] C. Pierre, J. Bouyssier, F. de Gournay, and F. Plouraboué. Numerical computation of 3D heat transfer in complex parallel heat exchangers using generalized Graetz modes. *J. Comp. Phys*, 268 :84–105, 2014.

[12] C. Pierre, J. Bouyssier, and F. Plouraboué. Mathematical analysis of parallel convective exchangers. *Math. Models and Methods Appl. Sci.*, 24(4) :627–667, 2013.

[13] C. Pierre and F. Plouraboué. Numerical analysis of a new mixed-formulation for eigenvalue convection-diffusion problems. *SIAM. J. Appl. Math*, 70 :658–676, 2009.

[14] A. E. Quintero, M. Vera, and B. Rivero-de Aguilar. Wall conduction effects in laminar counterflow parallel-plate heat exchangers. *Int. J. Heat Mass Transfer*, 70(1-3) :939–953, 2014.

[15] R. K. Shah and Dušan P. Sekulić. *Fundamentals of heat exchanger design*. John Wiley and Sons, New Jersey, 2003.

[16] Singh S.N. Heat transfer by laminar flow in a cylindrical tube. *Appl. Sci. Res.*, A7 :325 ?340, 1958.

[17] Wen-Quan Tao, Zeng-Yuan Guo, and Bu-Xuan Wang. Field synergy principle for enhancing convective heat transfer ? ?its extension and numerical verifications. *Int. J. Heat Mass Transfer*, 45(18) :3849–3856, 2002.

[18] M. Vera and A. Liñán. Laminar counter flow parallel-plate heat exchangers : Exact and approximate solutions. *Int. J. Heat Mass Transfer*, 53 :4885–4898, 2010.

[19] M. Vera and A. Liñán. Exact solution for the conjugate fluid-fluid problem in the thermal entrance region of laminar counter-flow heat exchangers. *Int. J. Heat Mass Transfer*, 54(1-3) :490–499, 2011.

[20] Qu W. and Mudawar I. Experimental and numerical study of pressure drop and heat transfer in a single-phase micro-channel heat sink. *Int. J. Heat Mass Transfer*, 45 :2549 ?2565, 2002.

[21] B. Weigand, M. Kanzamar, and H. Beer. The extended Graetz problem with piecewise constant wall heat flux for pipe and channel flows. *Int. J. Heat Mass Transfer*, 44(20) :3941–3952, 2003.

[22] B Weigand and D Lauffer. The extended Graetz problem with piecewise constant wall temperature for pipe and channel flows. *Int. J. Heat Mass Transfer*, 24 :5303–5312, 2004.

[23] H. Zhang and A. Lorente, S. Bejan. Vascularization with line-to-line trees in counterflow heat exchange. *Int. J. Heat Mass Transfer*, 52(19-20) :4327–4342, 2009.